Research Article | Vol. 29, No. 12 / 7 June 2021 / Optics Express 18743
Optics EXPRESS

2048-QAM transmission at 15 GBd over 100 km using geometric constellation shaping

YUTA WAKAYAMA,[1,4,*] THOMAS GERARD,[2,4] ERIC SILLEKENS,[2] LÍDIA GALDINO,[2] DOMANIÇ LAVERY,[2,3] ROBERT I. KILLEY,[2] AND POLINA BAYVEL[2]

[1]KDDI Research, Inc., 2-1-15 Ohara, Fujimino 356-8502, Japan
[2]Optical Networks Group, Department of Electronic and Electrical Engineering, University College London (UCL), Torrington Place, London WC1E 7JE, United Kingdom
[3]Infinera Canada Inc, Ottawa, ON K2K 2X3, Canada
[4]These authors contributed equally to this work
[*]yu-wakayama@kddi-research.jp

Abstract: We experimentally investigated a pilot-aided digital signal processing (DSP) chain in combination with high-order geometric constellation shaping to increase the achievable information rates (AIRs) in standard intradyne coherent transmission systems. We show that the AIR of our system at 15 GBd was maximised using geometrically-shaped (GS) 2048 quadrature amplitude modulation (QAM), reaching 18.0 b/4D-symbol in back-to-back transmission and 16.9 b/4D-symbol after transmission through 100 km of a single-mode fibre after subtracting the pilot overhead (OH). This represents the highest-order GS format demonstrated to date, supporting the highest AIR of any standard intradyne system using conventional optics and 8-bit electronics. Detailed characterisation of the DSP, transceiver performance, and transmission modelling has also been carried out to provide insight into sources of impairments and directions for further improvement.

1. Introduction

Information rates in coherent optical communication systems can be increased by using high-order quadrature amplitude modulation (QAM) formats, provided that the transmission system has a sufficient signal-to-noise ratio (SNR) [1,2]. The noise in the complete transmission system can be considered separately in the optical and electrical domains. In the optical domain, the transceiver SNR may be limited by phase noise from the transmitter and local oscillator lasers. Phase noise can limit information rates by reducing the accuracy of carrier phase recovery methods required in conventional intradyne coherent detection. This is particularly significant in systems with low symbol rates, as phase noise variance is proportional to the sample period used [3]. In the electrical domain, quantisation noise, thermal noise and clock jitter (to give a few examples) limit the effective number of bits (ENoBs) of digital-to-analogue converters (DACs) and analogue-to-digital converters (ADCs) [4–6]. In particular, finite clock jitter causes the ENoBs of electrical DACs and ADCs to decrease as the symbol rate increases; this has been shown to proportionally decrease the information rates and transmission capacities of systems with high symbol rates [7,8].

The combined impact of these noise sources determines the maximum SNR of a transmission system as a function of the symbol rate, defining the upper bound on the potential information rate. As an example, Fig. 1 shows the maximum information rate of a transceiver in the back-to-back configuration using parameters that are typical of our testbed (black solid curve): a linewidth symbol time product (LSTP) of 8.7×10^{-6} (two independent 65 kHz Lorentzian

#423361 https://doi.org/10.1364/OE.423361
Journal © 2021 Received 23 Feb 2021; revised 20 May 2021; accepted 24 May 2021; published 1 Jun 2021

Optics EXPRESS

linewidth lasers at 15 GBd), a maximum optical signal-to-noise ratio (OSNR) of 43 dB, and a combined intrinsic electrical timing jitter from a DAC and an ADC with 150 fs [9,10]. Note that the noise contributions are example values for illustration and that practical systems will also be limited by electrical noise and component nonlinearity. For symbol rates below 10 GBd, laser phase noise limits the SNR and, therefore, the achievable information rate (AIR). At symbol rates above 30 GBd, the decreasing ENoB of the electrical DACs and ADCs sets the limit on performance. Between 10 and 30 GBd, a region of interest exists for system operators who aim to maximise information rates while reducing the cost per bit by minimising the transceiver count.

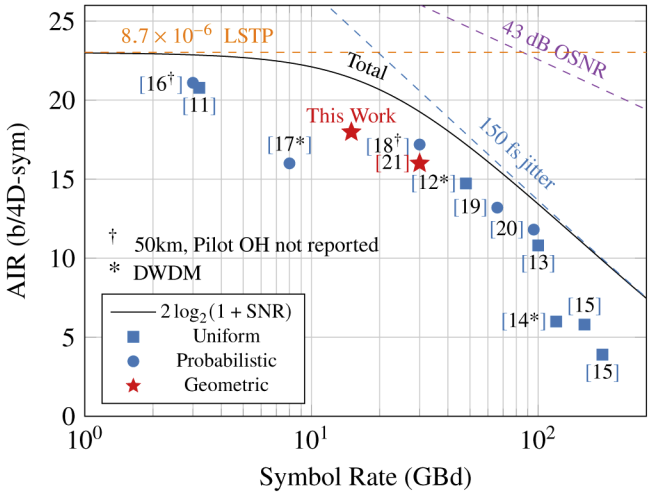

Fig. 1. Achievable information rate (AIR) vs. symbol rate in standard intradyne coherent transmission systems. The maximum AIR is bounded by transceiver noise, modelled here using example values from our system. The published AIRs for back-to-back setups are shown as markers, defined as the generalised mutual information (GMI) after deducting the pilot overhead (OH) and assuming an ideal-rate FEC, unless otherwise stated. The channels tested in dense wavelength division multiplexing (DWDM) setups are indicated.

Figure 1 also shows the state-of-the-art results obtained using standard intradyne coherent systems [11–21]. Each point represents the maximum reported single-channel AIR for that publication in the back-to-back scenario, unless otherwise stated. For publications that only reported bit error rates, the generalised mutual information (GMI) was simulated using Monte Carlo methods by assuming an additive white Gaussian noise channel. The highest information rates can only be achieved by reducing the impact of laser phase noise, which becomes increasingly significant below 30 GBd. Low phase noise is necessary to support high-order QAM formats, which can tolerate only relatively small, untracked variations in phase. An optical phase-locked loop (OPLL) can be used to reduce laser phase noise by seeding the local oscillator with a co-propagated out-of-band optical pilot tone [22–25]. However, this method consumes additional optical bandwidth, limiting the minimum channel spacing, and requires hardware architectures that differ from the commercially available, standard configurations.

Conversely, pilot-aided digital signal processing (DSP) allows for the implementation of high-order QAM in standard intradyne configurations [16,17,19]. In this scheme, known digital pilot symbols are embedded within the data payload and then extracted by DSP at the receiver for data-aided channel estimation. This approach does not impose a limit on the minimum channel spacing (in contrast to the OPLL method) and enables effective equalisation and carrier phase recovery with low computational complexity [26,27]. However, although the use of pilot symbols can improve the GMI of a channel, each pilot symbol replaces a payload transmission

Optics EXPRESS

symbol, thereby reducing the information rate. Therefore, these contributions must be balanced to maximise the AIR, which is defined here as the GMI minus the pilot overhead (OH), and they assume an ideal-rate, binary, soft-decision, forward error correction (FEC) code.

A key advantage of performing channel estimation using only pilot symbols is that the payload can be mapped using arbitrary constellation schemes with minimal implementation penalties. This has enabled the practical use of probabilistically-shaped (PS) and geometrically-shaped (GS) constellations, which can be designed to maximise the GMI for a given SNR. Probabilistic shaping adjusts the occurrence rates of individual square-QAM symbols, while geometric shaping shifts the target symbol positions in the complex plane. It has been shown that a 2-dimensional (2D) PS constellation is able to approach the Shannon limit under the assumption of infinitely long block lengths, even for low-order QAM formats [28]. PS formats have therefore been applied in numerous demonstrations to increase their AIRs by 0.5-0.9 b/4D-symbol (b/4D-sym) [16,18–20]. However, the PS multi-symbol (de)mapping algorithm is computationally expensive and power hungry, and the channel performance varies with the block length [29]. In contrast, GS constellations can use conventional (de)mapping procedures with no additional computational OH and offer GMI gains for any block length [28,30]. This makes the performance of GS formats competitive with that of PS formats in practical transmission systems [31]. While low-order GS formats have been shown to offer modest shaping gains of <0.3 b/4D-sym [32], recent work has demonstrated that GS-1024 QAM can achieve gains of 0.7 b/4D-sym, reaching an AIR of 17.4 b/4D-sym at 15 GBd in a back-to-back configuration [21]. Pilot-aided GS high-order QAM is, therefore, a promising technique for low-complexity, high-AIR transmission systems.

This paper extends on the work presented in [21] by investigating the application of pilot-aided GS high-order QAM to maximise the AIRs of short-distance transmission systems. A symbol rate of 15 GBd is targeted to balance the phase noise and jitter contributions. Through detailed calibration of the pilot DSP chain, SNRs as high as 29.5 dB were demonstrated to support constellations as large as 2048 QAM. A gradient descent algorithm was used to optimise the GMI of GS-2048 QAM, shown to exceed the AIR of GS-1024 QAM at the SNRs under consideration when evaluated using a standard intradyne transmission system composed of 65 kHz linewidth lasers, 8-bit DACs/ADCs, erbium-doped fibre amplifiers (EDFAs), and 100 km of low-loss, single-mode fibre. We show that the AIR of GS-2048 QAM at 15 GBd can be increased to as much as 18.0 b/4D-sym, which is the highest AIR of any standard intradyne 8-bit coherent transceiver reported to date.

2. Experimental setup

The experimental setup is shown in Fig. 2(a). An external cavity laser (ECL) emitting at 193.4 THz (1550 nm) was modulated by an Oclaro (now Lumentum) dual-polarisation (DP) IQ modulator. The linewidth of the ECL was estimated by mixing the unmodulated output with a narrow-linewidth (rated <1 kHz) test source, offset by 2 GHz, and measuring the beat signal using a digital coherent receiver. An ideal Lorentzian lineshape was then fitted to the beat signal using least mean squares regression, giving a linewidth estimate of 65 kHz. The modulator was driven by a 92-GSa/s 8-bit DAC with 32-GHz analogue bandwidth, supported by linear amplifiers with 55-GHz electrical bandwidth. The modulated optical signal was followed by an EDFA and a variable optical attenuator (VOA) to control the launch power of the transmitter. The signal was then transmitted through 100 km of Corning Vascade EX2000 single-mode fibre (SMF) with a total loss of 16 dB [33]. Before the receiver, the signal was coupled with an amplified spontaneous emission (ASE) source and VOA to vary the received OSNR, up to a maximum of 43 dB (noise bandwidth: 0.1 nm). The signal was coherently detected using a polarisation-diverse optical 90-degree hybrid, 70-GHz balanced photodetectors, and an 8-bit 63-GHz-bandwidth digital sampling oscilloscope operating at 160 GSa/s [21]. At a symbol rate of 15 GBd, the ENoBs of the DAC and ADC were measured as 5.0 bits and 4.8 bits, respectively [6,7].

Optics EXPRESS

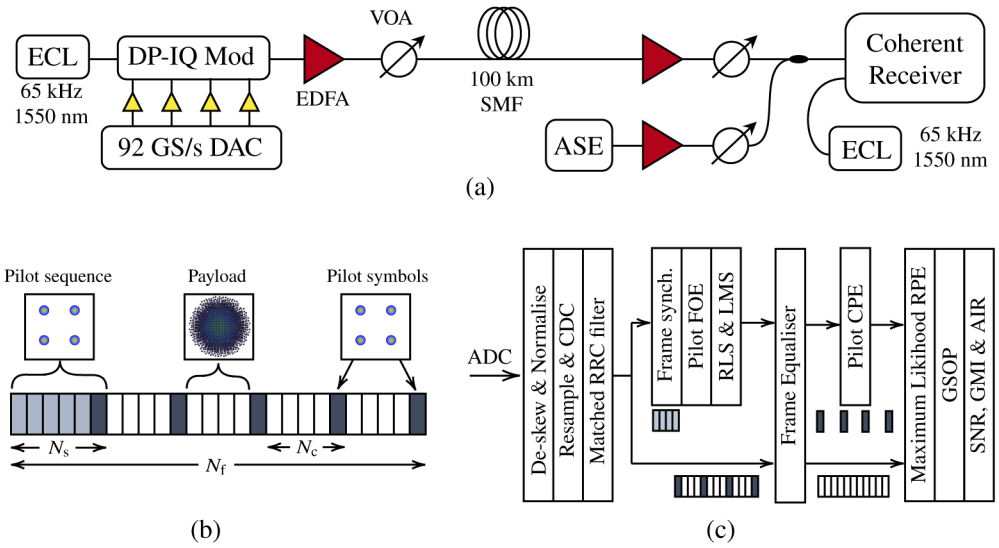

Fig. 2. (a) Experimental setup. (b) Structure of the pilot-aided transmission frame. Each payload is preceded by a pilot sequence with a length of N_s and interleaved with pilot symbols once every N_c symbols. (c) Receiver-side DSP chain.

To show the benefit of GS-2048 QAM, the performance of 64 256, 1024, 2048, GS-1024 and GS-2048 QAM was characterised. The GS constellations were designed by mapping random information bits to each initially square format and then iteratively perturbing the complex coordinates of the constellation points to change the GMI. A gradient descent algorithm was used to find the optimal constellation coordinates that maximised the GMI at an SNR of 28 dB for both 1024- and 2048-*ary* constellations, while assuming an additive white Gaussian noise (AWGN) channel. The GMI was chosen as the target metric because it provides an upper bound for the information rate under the assumption of a binary soft-decision decoder [34]. Due to the size of the constellation, it was computationally infeasible to reassign the bit-to-symbol mapping during each optimisation step [35], so the optimisation algorithm was instead initialised with Gray-labelled uniform QAM, known to be a good mapping approach at high SNRs. The optimised constellations for GS-1024 QAM and GS-2048 QAM are shown in Figs. 3(a) and (b), respectively.

Before it was uploaded to the DAC, the signal was spectrally shaped with a root-raised cosine filter (roll-off: 0.01) and nonlinear pre-emphasis [36]. Quadrature phase shift keying (QPSK) pilot symbols were embedded within the data payload to construct a data frame, as shown in Fig. 2(b). The power of the pilot symbols was set to match that of the payload symbols. Each frame was preceded by a QPSK pilot sequence of length N_s that was used for frame synchronisation and equalisation [26]. Thereafter, individual pilot symbols were inserted at a pilot rate of ${N_c}^{-1}$ within the payload, and these were used for carrier phase estimation (CPE). The complete frame size was N_f, such that the pilot OH is defined as

$$[N_s + (N_f - N_s)/N_c]/N_f. \tag{1}$$

The receiver DSP chain is shown in Fig. 2(c). The received signal was compensated for receiver skew, normalised, and then resampled to 2 samples/symbol. In the transmission case, chromatic dispersion compensation was then applied based on the frequency domain overlap-and-add method [37]. After matched filtering, the pilot sequence was isolated using the minimum error terms of an 11-tap equaliser based on the constant modulus algorithm (CMA); fine alignment of

Optics EXPRESS

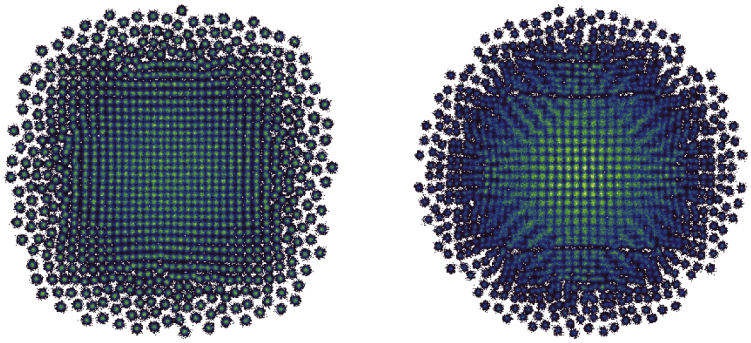

Fig. 3. The geometrically-shaped (GS) constellation diagrams used in this work: (a) GS-1024 QAM and (b) GS-2048 QAM. The complex coordinates of each format were optimised through gradient descent to maximise the GMI for an SNR of 28 dB.

the complete frame was then carried out by performing cross correlation on the received and expected pilot sequence waveforms [38]. The isolated pilot sequence was used for data-aided frequency offset estimation (FOE), the results of which were applied to all of the received samples. Following this, the pilot sequence was used for data-aided channel estimation by training an 11-tap finite impulse response adaptive equaliser using two sequential algorithms. First, the recursive least squares (RLS) algorithm was applied; it was selected because of its fast convergence time [39]. Second, the pilot sequence symbols were passed to the least mean squares (LMS) algorithm with progressively smaller learning parameters to reduce the final error of the inverse channel estimate. The trained equaliser taps were then applied to the rest of the received samples (containing the data payload as well as the embedded pilot symbols) with no further updates to the tap values. Following equalisation, the pilot symbols embedded within the payload were extracted based on their known symbol locations, and a two-step CPE algorithm was implemented. In the first step, the phase noise of the pilot symbols was estimated by comparing their received and known complex arguments, beginning with the last symbol of the pilot sequence. The progression of the carrier phase throughout the frame was then estimated by linear interpolation between neighbouring pilot symbols, as described in [40], compensating for the majority of the phase noise. The second step of CPE applied a maximum-likelihood (ML) estimator based on that described in [41] (with a length of $N_c/2$) to the payload symbols, serving as a residual phase noise estimator (RPE). This permitted our system to tolerate larger values of N_c, thereby decreasing the pilot OH. Finally, after applying the Gram-Schmidt orthogonalisation procedure (GSOP) described in [42], the recovered payload symbols were used to estimate the SNR and GMI, and the AIR was calculated by deducting the pilot OH from the GMI using Eq. (1). Note that the OH depends on the frame length N_f and, in our experiment, it was limited by the DAC memory size to $N_f \approx 2^{16}$ at 15 GBd.

3. Results and discussion

3.1. Pilot-aided DSP calibration

The use of pilot symbol parameters must be optimised to balance the trade-off between GMI improvements and penalties from increased pilot OH. The appropriate selection of N_s and N_c is system specific and can depend on the modulation format, symbol rate, received SNR, linewidth and nonlinear impairments [40,43,44]. In this work, we followed the approach established in [38], where N_s and N_c were varied and the GMI was measured to maximise the resultant AIR. The optimisation results obtained using our system for 64, 256, 1024 and GS-1024 QAM can

Optics EXPRESS

be found in [21]; here, we extended that work to focus on the optimisation of 2048 QAM and GS-2048 QAM to explore how pilot requirements vary in high-order GS transmission systems.

To determine the optimal pilot sequence length, N_s was swept from 2^7 to 2^{14} symbols for both 2048 and GS-2048 QAM. N_f and N_c were kept at the 2^{16} and 2^5 symbols, respectively. The GMI and AIR were measured and are shown in Fig. 4. For both formats, the GMI was weakly dependent on N_s for sequences between 2^7 and 2^{11}, although GS-2048 QAM did exhibit a peak GMI of 18.9 b/4D-sym at $N_s = 2^9$. The AIR values for both formats were observed to degrade for sequence lengths of $N_s = 2^{10}$ and greater. This is because the pilot OH took up an increasingly significant proportion of the data frame, limiting its useful throughput. GS-2048 QAM peaked at an AIR of 18.2 b/4D-sym for $N_s = 2^9$, while 2048 QAM peaked at 16.9 b/4D-sym for $N_s = 2^8$. The results indicate that just a few hundred data-aided symbols are required for accurate laser frequency offset calculation and channel estimation. In the following sections, we adopt a pilot sequence length of 2^{10}, providing close to optimal performance while creating resilience to variations in the above system imperfections.

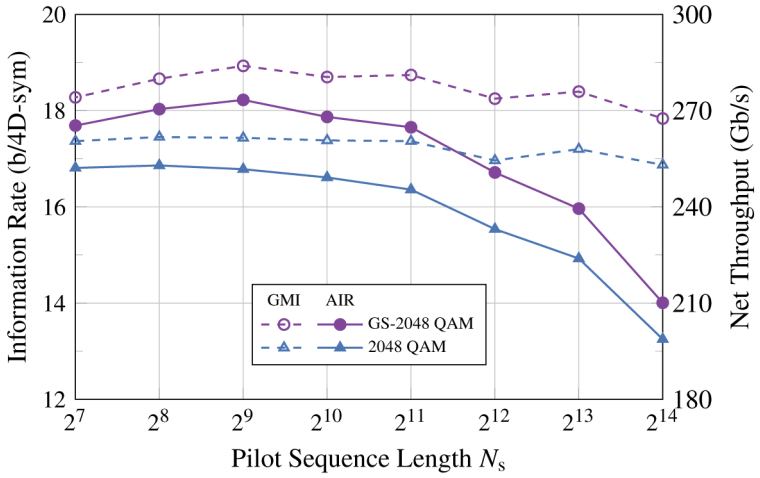

Fig. 4. Effect of the pilot sequence length on the information rates for back-to-back 15 GBd transmission ($N_c = 2^5$, $N_f = 2^{16}$).

To determine the optimal pilot symbol length for effective CPE, N_c was swept from 2 to 2^9 symbols for both 2048 and GS-2048 QAM. N_f and N_s were kept at 2^{16} and 2^{10} symbols, respectively. The measured GMI and AIR are shown in Fig. 5. The greatest GMI values for both formats were observed for $N_c = 2$; here, our system SNR exceeded 30 dB, and the GS-2048 QAM format reached a GMI of 19.1 b/4D-sym. However, $N_c = 2$ represents a pilot being placed at every other symbol; this seriously limits the AIR and so is undesirable in practical transmission systems. For values of $N_c > 2^7$, both the GMI and the AIR were observed to sharply decrease due to the inaccuracy of the CPE. The maximum AIRs for both 2048 and GS-2048 QAM were measured at 2^6, peaking at 16.9 and 18.1 b/4D-sym, respectively. It is interesting to note that the GMI of both 2048 and GS-2048 QAM decreased by approximately 0.5 b/4D-sym when N_c was increased from the optimal GMI value of 2 to the optimal AIR value of 2^6. This represents a drop from the maximum system SNR of ~ 1 dB, which can be directly attributed to inaccuracies in the CPE methods applied here. This indicates that residual phase noise still represents a limiting factor in our system and that further AIR gains can be achieved through its mitigation. We note that phase noise-aware geometric shaping and decision thresholds have been shown in simulations to reduce the impact of residual phase noise in pilot-aided systems [45]. Future work could therefore apply these techniques to achieve improved AIR performance with minimal

Optics EXPRESS

increases in DSP complexity. For the remainder of this paper, we adopt a conservative pilot symbol block length of $N_c = 2^5$, giving us close-to-optimal CPE performance while providing the system resilience to variations in laser phase noise and frequency offset.

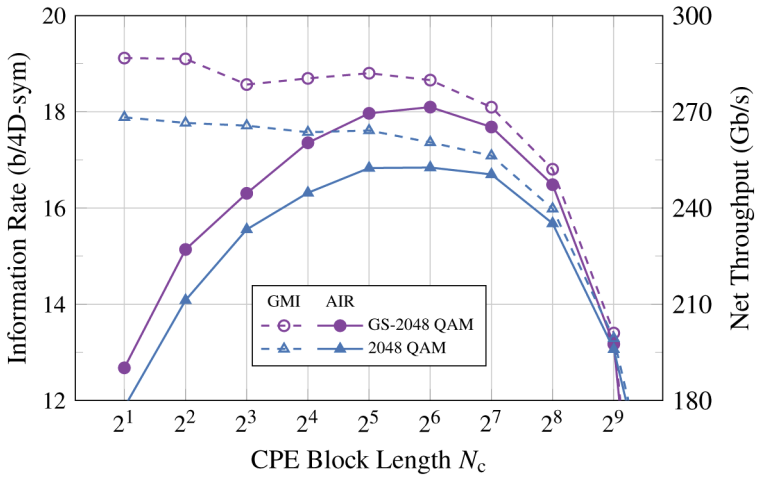

Fig. 5. Effect of the pilot symbol block length on the resulting information rates for back-to-back 15 GBd transmission ($N_s = 2^{10}$, $N_f = 2^{16}$).

3.2. Back-to-back transceiver characterisation

Using the pilot parameters determined above ($N_s = 2^{10}$, $N_c = 2^5$, $N_f = 2^{16}$, and OH = 4.64%), back-to-back noise loading was performed to measure the maximum experimental transceiver SNR together with the implementation penalties. The OSNR was varied using the ASE source, and the SNR was measured for both 2048 and GS-2048 QAM. The results are shown in Fig. 6. Assuming that the noise contributions are statistically independent, the total SNR of the back-to-back system can be modelled as

$$\frac{1}{\mathrm{SNR}_{\mathrm{BtB}}} = \frac{1}{\mathrm{SNR}_{\mathrm{ASE}}} + \frac{1}{\mathrm{SNR}_{\mathrm{TRX}}}, \tag{2}$$

where $\mathrm{SNR}_{\mathrm{ASE}}$ is the SNR constrained by ASE noise and $\mathrm{SNR}_{\mathrm{TRX}}$ is the SNR constrained by the transceiver [6]. The ideal limit of $\mathrm{SNR}_{\mathrm{BtB}}$ for a given OSNR over a bandwidth of 0.1 nm is shown in Fig. 6 as a solid line assuming an ideal transceiver ($\mathrm{SNR}_{\mathrm{TRX}} = \infty$). In this case, $\mathrm{SNR}_{\mathrm{BtB}}$ is simply given by $\mathrm{SNR}_{\mathrm{BtB}} = \mathrm{OSNR} - 10\log_{10}(R_s/B_n)$, where R_s is the symbol rate and B_n is the noise bandwidth. The left inset shows that in the low-OSNR region where ASE dominates, the experimental results for both 2048 and GS-2048 QAM approach the ideal limit (within 0.01 dB). As the OSNR increases, the measured formats diverge from the ideal limit because ASE is no longer the dominant noise source, and transceiver impairments become non-negligible. In this case, the non-ideal SNR limit can be modelled by evaluating Eq. (2) for a finite transceiver SNR of $\mathrm{SNR}_{\mathrm{TRX}} = 29.5$ dB. This is shown in Fig. 6 as a dashed curve. Both formats are observed to closely track the non-ideal SNR limit throughout the figure, indicating that our system suffers from no significant impairments outside of those described by Eq. (2) and that our pilot-aided transceiver SNR is 29.5 dB. The right inset in Fig. 6 shows the high-OSNR regime in more detail. We observe that the uniform 2048 QAM reaches a maximum measured value of $\mathrm{SNR}_{\mathrm{BtB}} = 29.5$ dB, slightly outperforming the GS-2048 QAM data, which has the best recorded result of 29.3 dB. The format-specific transceiver SNR can be measured by fitting the experimental data to the model given in Eq. (2) using least-squares regression. Fitting the datasets individually gives

Optics EXPRESS

a value of SNR_{TRX} = 29.53 dB for 2048 QAM and SNR_{TRX} = 29.46 dB for GS-2048 QAM. These results suggest that using the GS format has reduced the transceiver SNR by approximately 0.1 dB; this represents an OSNR penalty of 0.85 dB at the SNR_{BtB} = 29 dB level. This shaping penalty is attributed to small changes in the DAC peak-to-average-power ratio (PAPR) before and after shaping. The influence of the PAPR on performance was not considered when optimising the geometric constellations used in this work; however, previously, we demonstrated that this effect can be included [46].

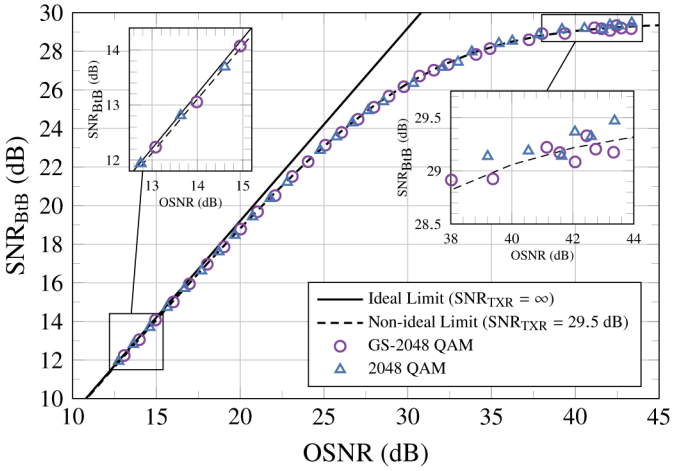

Fig. 6. Back-to-back noise loading to assess transceiver performance at 15 GBd ($N_s = 2^{10}$, $N_c = 2^5$, and $N_f = 2^{16}$) relative to a 0.1 nm noise bandwidth. SNR_{BtB} is the combined SNR and includes all noise contributions in the back-to-back configuration. SNR_{TRX} is the transceiver-constrained SNR.

Although the GS-2048 QAM format has been shown to reduce the maximum achievable system SNR, the information rate can still be increased by closing the gap to capacity. To quantify this, the simulated and experimental GMI results achieved for a given SNR are shown in Fig. 7. The simulation results were obtained offline through Monte Carlo analyses of the formats under examination. The results are shown for 1024 QAM, 2048 QAM, GS-1024 QAM and GS-2048 QAM to provide a complete comparison. The measured GMIs of the experimental data show good agreement with the simulated results for all formats, though an implementation penalty of $\lesssim$ 0.1 dB in terms of the SNR is observed throughout. This is attributed to the use of non-ideally Lorentzian lasers in the experiment, creating additional residual phase noise than that modelled in our simulation. Although the GS formats were shaped to optimise performance for a particular SNR (28 dB in this work), GMI gains over those of the uniform formats were observed for a wide range of SNR values. The maximum experimental GMI value measured using GS-2048 QAM was 18.82 b/4D-sym at an SNR of 29.3 dB; this exceeds the maximum GMI obtained using 2048 QAM, which was 18.59 b/4D-sym at an SNR of 29.5 dB. Therefore, despite the penalty to the maximum achievable SNR identified in Fig. 6, geometric shaping helped increase the maximum GMI of the experimental system by 0.23 b/4D-sym.

The geometric shaping gains across a range of SNR values are shown in Fig. 8(a); these were calculated by subtracting the GMI of the GS data from the GMI of the corresponding uniformly shaped data given in Fig. 7. The experimental data show good agreement with the simulation, where deviations are due to variations in the format-specific GMI penalty observed in Fig. 7. A peak gain of 0.69 b/4D-sym for GS-2048 QAM was observed in the simulated data at an SNR of 23.5 dB; this was confirmed by experiments up to 0.63 b/4D-sym. Greater gains could potentially be achieved by shaping specifically for this SNR; however, in this work, we focused on shaping

Optics EXPRESS

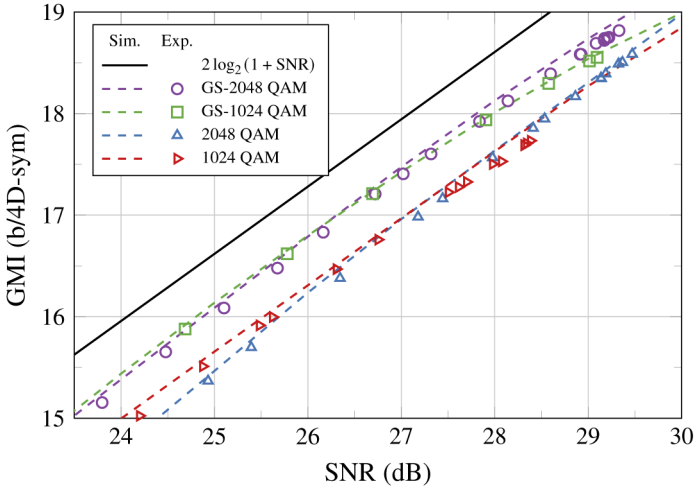

Fig. 7. Simulated and experimental GMI results for a given SNR in a pilot-aided DSP system ($N_s = 2^{10}$, $N_c = 2^5$, $N_f = 2^{16}$).

at greater SNR values to maximise information rates. At the optimised SNR of 28 dB, both GS-1024 QAM and GS-2048 QAM achieved GS gains of ~ 0.45 b/4D-sym; the gain decreased as the SNR increased further. This is because the GMI performance of all the formats under test began to saturate in the high-SNR regime, as explained below.

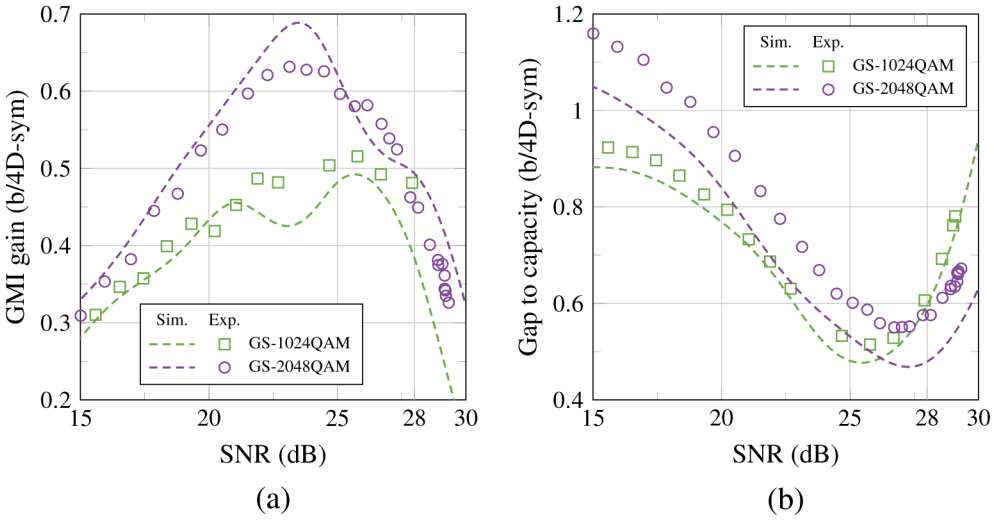

Fig. 8. (a) Gain in GMI achieved by geometrically shaping 1024 and 2048 QAM. (b) Gaps to capacity for GS-1024 QAM and GS-2048 QAM. Both GS constellations were optimised for an SNR of 28 dB.

Overall, these GMI gains for a given SNR permit our system to approach the Shannon limit. The gaps to capacity for the geometric shaping results are shown in Fig. 8(b); these were calculated by subtracting the simulated and experimental GMI results from the Shannon limit. The smallest gap occurred around SNR values of 25.5 dB for GS-1024 QAM and 27 dB for GS-2048 QAM. These optimal positions were lower than those targeted by our regression optimiser (28 dB). This occurred because the GMIs of both formats began to saturate, so the optimiser was not able to

Optics EXPRESS

further close the gap to capacity. This conclusion is supported by the fact that GS-2048 QAM experimentally outperformed GS-1024 QAM for SNRs greater than 27 dB, indicating that the lower cardinality of 1024 QAM approached peak performance. Similarly, the gap to capacity of GS-2048 QAM increased from 28 dB onwards, suggesting that it also has insufficient cardinality and that GS-4096 QAM may offer superior information rates at these higher SNRs. However, the transmission results in section 3.3 show that once the SNR penalties associated with transmission have been accounted for, GS-2048 QAM is the correct choice of format for our system. We note that Fig. 8(b) shows that the simulated gap to capacity was at best 0.48 b/4D-sym and experimentally verified down to 0.51 b/4D-sym. Previously, we showed that GS-1024 QAM, shaped for the AWGN channel, can theoretically approach capacity to within ~ 0.2 b/4D-sym [47]. The additional simulated gap of ~ 0.3 b/4D-sym is also caused by the saturation of the formats considered in this work, as they do not have sufficiently high cardinality to make full use of the high system SNR. Again, we expect that using GS-4096 QAM at these SNRs could offer a gap to capacity of ~ 0.2 b/4D-sim; this is discussed further in section 3.4.

It was highlighted above that the GS formats in Fig. 7 outperformed the uniform formats over a wide SNR range, despite being optimised for specific SNR targets. To quantify the range over which this is valid, Fig. 9 shows the complete experimental data for 64, 256, 1024, 2048, GS-1024 and GS-2048 QAM, where the GMI was calculated from the measured SNRs. As the pilot-aided DSP is responsible for all forms of signal recovery, we observed <0.5 dB of variation in the maximum achievable system SNR across all of the modulation formats tested. As is typical [2], due to the variation in bitwise encoding performance and the gradual saturation of the SNR for each format, different uniform QAM formats are needed to maximise the GMI as the SNR increases. Therefore, in a system with continuously adjustable FEC rates, the constellation cardinality should be increased as soon as a given format begins to saturate to maximise the GMI. This is shown in Fig. 10(a), where the uniform QAM format that maximises the GMI is given for each SNR. This is similar to the relationship between code rates and SNRs presented in [2], where the use of pilot-aided DSP has allowed us to (1) improve the maximum system SNR to 29 dB and (2) decouple the DSP performance from the modulation format. For example, when the SNR exceeds 16.7 dB, the modulation format should be changed from 64 QAM (using an ideal FEC rate of 0.855 with 17% OH) to 256 QAM (FEC rate of 0.645 with 55% OH) for optimal performance. We note that this same transition is given in Fig. 4 of [2] but occurring at slightly lower rate of 0.642 with 56% OH — this difference is caused by the pilot DSP chain used in this work, which offers improved performance as the QAM order increases.

However, the gains in GMI from geometric shaping create new optimal formats for the investigated transmission system. This is observed in Fig. 9, where the GS formats outperform the uniform formats for a wide range of SNR values. The format that maximises the GMI, now including GS-1024 and GS-2048 QAM, is shown in Fig. 10(b). GS-1024 QAM is the superior format between 18 dB and 27 dB, making uniform 1024 QAM superfluous. Indeed, any QAM format with higher cardinality can be shaped to achieve equivalent performance to that of a lower cardinality format, so long as the GMI of either format has not saturated. Therefore, the higher cardinality format is only truly justified if the system SNR is high enough such that the lower cardinality format starts to saturate. Therefore, in this work, the use of GS-2048 QAM can be justified as long as the system SNR is maintained at 27 dB or higher.

3.3. Transmission results

For the transmission experiment, a signal was passed through 100 km of SMF, re-amplified using an EDFA, and then received using a DP coherent receiver. The launch power was varied, and the SNR was measured to balance the linear and non-linear penalties; the experimental results are shown in Fig. 11. The expected performance was also calculated using the Gaussian noise (GN) model. For the single transmission span considered here, the total SNR after chromatic

Optics EXPRESS

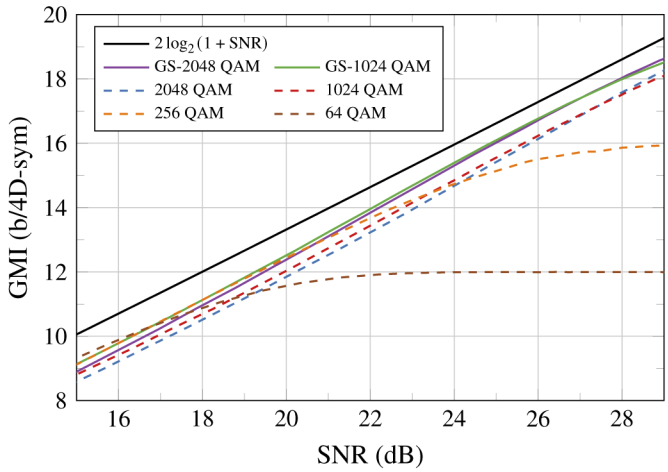

Fig. 9. Experimental GMI results for a given SNR in a pilot-aided DSP system ($N_s = 2^{10}$, $N_c = 2^5$, $N_f = 2^{16}$).

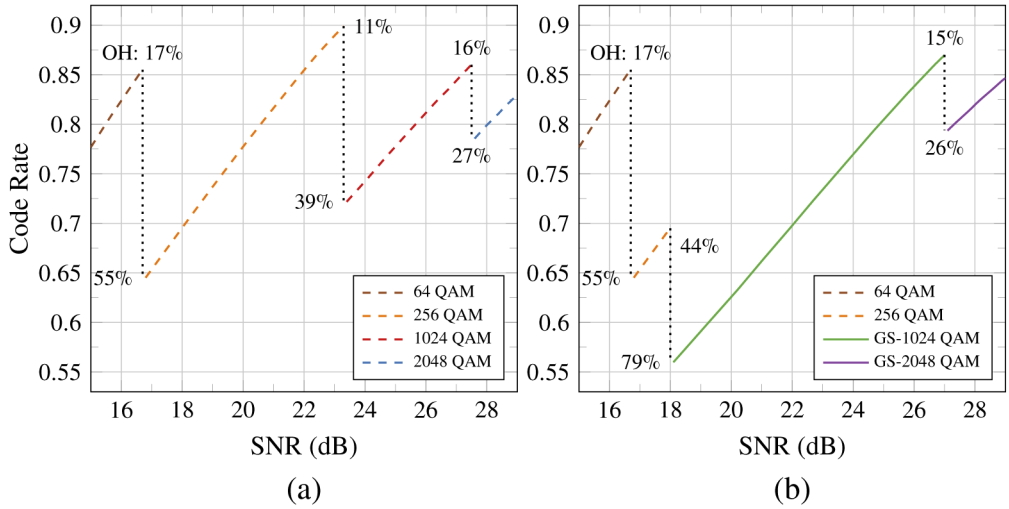

Fig. 10. The optimal modulation format as a function of the received SNR in a pilot-aided DSP transmission system, assuming continuously adjustable FEC rates. (a) Uniform QAM formats only. (b) GS QAM formats included. FEC OHs are related to the code rate, R_c, by $\text{OH} = 1/R_c - 1$. The dotted lines indicate the points at which the modulation format should be changed to maximise the information rate.

dispersion compensation is given by

$$\text{SNR}_{\text{Total}} = \frac{P}{\kappa P + P_{\text{ASE}} + \eta_1 P^3}, \tag{3}$$

where P is the launch power, κ represents the power-independent noise contributions, P_{ASE} is the ASE noise power within the channel bandwidth, and η_1 is the nonlinear interference coefficient after one span. Guided acoustic-wave Brillouin scattering (GAWBS) describes how a propagated optical signal is scattered by thermally-induced acoustic modes in the radial direction [48] and has been shown to introduce a non-negligible penalty in the transmission of high-SNR

Optics EXPRESS

and high-cardinality signals even over relatively short distances compared to those of subsea cables [49]. Following the approach suggested in [49,50], we define $\kappa = 1/\mathrm{SNR}_{\mathrm{TRX}} + \gamma_{\mathrm{GAWBS}}L$, where γ_{GAWBS} is the GAWBS coefficient and L is the transmission distance. $\mathrm{SNR}_{\mathrm{TRX}}$ was set to 29.5 dB, as experimentally measured in section 3.2. γ_{GAWBS} was calculated as −28.7 dB/Mm using the closed-form expression given in Eq. (6) of [51] considering an SMF with an average effective area of 112 $\mu\mathrm{m}^2$, as used in this experiment. The GAWBS contribution after 100 km of transmission was therefore −38.7 dB, giving a final value of $\kappa = -29.0$ dB. P_{ASE} was set as −36.2 dBm, calculated using the relationship $P_{\mathrm{ASE}} = GF_{\mathrm{n}}h\nu R_{\mathrm{b}}$, where G is the EDFA gain (set equal to αL, where α is the fibre loss coefficient), F_{n} is the EDFA noise figure (5 dB), h is Planck's constant and ν is the central frequency of the channel (193.4 THz) [52]. η_1 was set equal to 140 W^{-2}, calculated using the closed-form expression derived in [53], a fibre loss coefficient of 0.16 dB km^{-1}, a group velocity dispersion of 25.75 $\mathrm{ps}^2\mathrm{km}^{-1}$, and a nonlinear coefficient of 0.85 $\mathrm{W}^{-1}\mathrm{km}^{-1}$. The modelled performance is shown in Fig. 11.

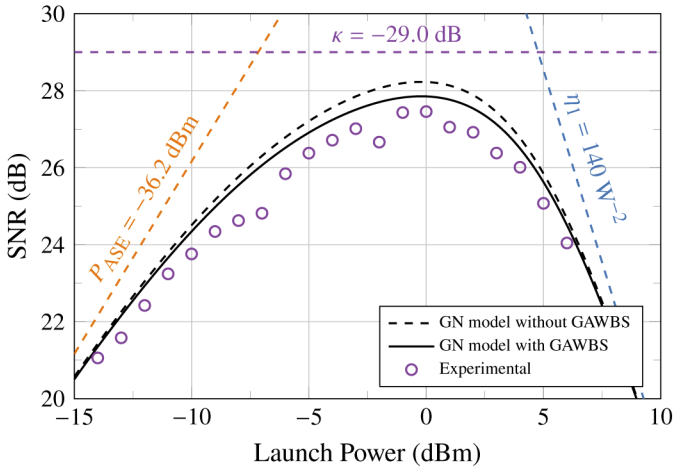

Fig. 11. Effect of launch power on the received SNR after 100 km of low-loss SMF transmission.

Good agreement is observed between the modelled and experimental results at both low and high launch powers, where finite OSNRs and non-linear effects dominate, respectively. These contributions predict an optimal launch power of 0 dBm, which is in agreement with the experimental data. At the optimal launch power, the peak modelled SNR was decreased by 0.4 dB due to the inclusion of GAWBS inference, corresponding to a penalty of 0.2 b/4D-sym. The peak experimental SNR of 27.5 dB fell short of that of the GN model with GAWBS by a further 0.4 dB; again, this is estimated to reduce the system GMI by 0.2 b/4D-sym. This discrepancy is attributed to measurement error and model imperfections.

Despite this penalty, an SNR of 27.5 dB after 100 km of transmission is still sufficient to justify the use of GS-2048 QAM, as determined in Fig. 10(b). Furthermore, an SNR of 27.5 dB is where GS-2048 QAM experiences the smallest gap to capacity, as seen in Fig. 8(b). Of the formats considered in this work, GS-2048 QAM is therefore the format that is able to maximise the AIR at this SNR and is thus the correct choice for the transmission experiment. Figure 12 summarises the back-to-back and transmission results presented in this paper in terms of (a) the normalised GMI (NGMI) and (b) AIR. Here, the NGMI is defined as the measured GMI divided by $2\log_2(M)$, where M is the constellation cardinality. It has previously been shown that the NGMI is the appropriate measure for predicting the performance of a soft-decision FEC decoder independent of the modulation format [34].

Optics EXPRESS

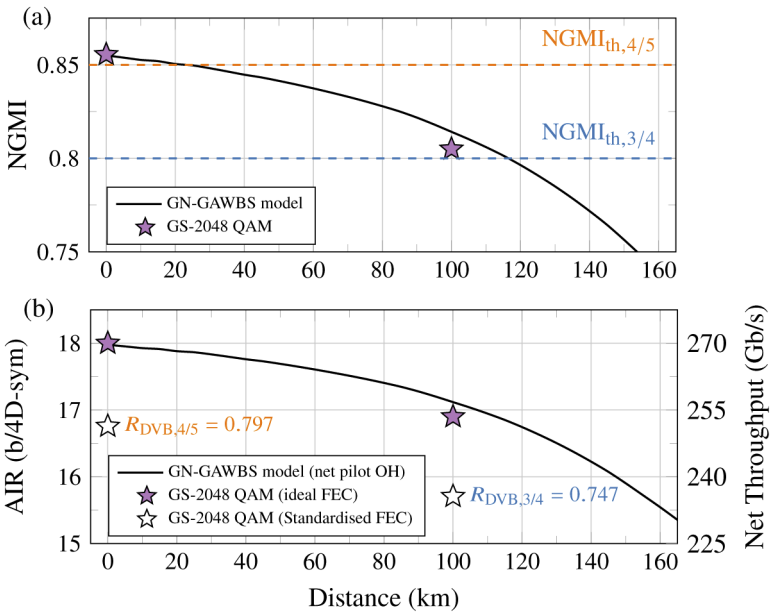

Fig. 12. (a) Normalised GMI vs. distance. The NGMI thresholds $\text{NGMI}_{\text{th},R_c}$ for achieving successful decoding using two example standardised FEC rates from the DVB standard, $R_c = 4/5$ and $R_c = 3/4$, are shown as dotted lines. (b) AIR vs. distance after subtracting FEC and pilot OHs. The AIR for the example DVB FEC rates correspond to the thresholds in (a).

In the ideal case, the FEC code rate matches the NGMI of the received signal, and thus the total SNR is used to support the transfer of useful information with no additional margin. Figure 12(a) shows that the back-to-back system using GS-2048 QAM at 15 GBd supports an NGMI of 0.8554; this degrades to 0.8052 after 100 km. The ideal degradation predicted using the GN model with GAWBS is shown for comparison, assuming unrepeatered transmission. The corresponding AIR for each point is shown in Fig. 12(b), with a deducted pilot OH of 4.64%. Before transmission, GS-2048 QAM supports 18.0 b/4D-sym at 15 GBd for a net throughput of 269.7 Gb/s. This is the highest AIR reported to date using standard intradyne coherent detection supported by 8-bit DACs and ADCs, outperforming previous 8-bit demonstrations that use lower symbol rates [17]. After 100 km, the system supports 16.9 b/4D-sym for a net throughput of 253.9 Gb/s. This AIR outperforms that of PS-4096 QAM transmitted over 50.9 km at 30 GBd using 1 kHz linewidth lasers [18]. These results demonstrate that higher-order GS QAM, aided by pilot DSP, can be used to achieve exceptionally high information rates even while using conventional receivers, lasers, fibres and amplifiers typical of deployed intradyne coherent transmission links. Furthermore, these results indicate that high-order GS QAM can perform competitively with PS constellations while using a lower complexity (de)mapping procedure that could potentially reduce line system cost and power consumption.

Although the above analysis assumed an ideal FEC rate, the information given in Fig. 12 is sufficient to calculate the AIR for any given off-the-shelf FEC code. As an example, here, we consider the application of the low-density parity check (LDPC) FEC codes defined in the 2$^{\text{nd}}$ generation European digital video broadcasting (DVB) standard [54]. These codes apply an inner soft-decision LDPC code and an outer hard-decision Bose-Chaudhuri-Hocquenghem (BCH) code for post-FEC bit error rates below 10^{-12}. For a given inner LDPC code rate $R_c \in \{1/4, 1/3, 2/5, 1/2, 3/5, 2/3, 3/4, 4/5, 5/6, 8/9, 9/10\}$, the NGMI threshold required for

Optics EXPRESS

successful decoding can be conservatively estimated as $\mathrm{NGMI}_{\mathrm{th},R_c} = R_c + 0.05$ [34]. The NGMI thresholds appropriate for our results are shown in Fig. 12(a). For $R_c = 4/5$, our back-to-back result exceeds $\mathrm{NGMI}_{\mathrm{th},4/5} = 0.85$. At this rate, the DVB standard encodes 51648 information bits into a 64800 bit frame for a combined LDPC-BCH rate of $R_{\mathrm{DVB},4/5} = 0.797$. The AIR can then be calculated using the relation $R_{\mathrm{DVB},R_c} m/(1 + \mathrm{OH})$, where m is the nominal number of bits per 4D-sym ($2\log_2(M)$ for DP M-ary QAM) and OH is the pilot OH given by Eq. (1). Therefore, the AIR for our back-to-back GS-2048 QAM result using $R_{\mathrm{DVB},4/5} = 0.797$ and OH = 0.0464 is $0.797 \cdot 22/1.0464 = 16.8$ b/4D-sym at 15 GBd, supporting a net throughput of 251.3 Gb/s. Similarly, for $R_c = 3/4$, our 100-km result exceeds $\mathrm{NGMI}_{\mathrm{th},3/4} = 0.80$. At this rate, 48408 information bits are encoded into a 64800 bit frame for a combined LDPC-BCH rate of $R_{\mathrm{DVB},3/4} = 0.747$. After subtracting the pilot OH, the AIR using this specific FEC scheme is 15.7 b/4D-sym at 15 GBd, supporting a net throughput of 235.6 Gb/s.

3.4. System limitations and directions for improvement

The pilot-aided DSP chain presented in this work has allowed our 8-bit transmission system to reach exceptionally high SNRs, enabling record high AIRs while justifying the use of the highest GS cardinality in an optical fibre channel reported to date. However, our analysis has indicated several areas of improvement that could lead to even higher information rates:

1. The characterisation of the pilot symbol CPE block length N_c presented in Fig. 5 indicated that 0.5 b/4D-sym was lost to imperfect phase noise tracking. This shows that residual phase noise is still present in the signal after CPE, and this can in principle be further reduced. This performance could be regained through improved CPE methods, as well as the use of phase noise-aware geometric shaping and demappers [45,55–57].

2. The simulation and experimental SNR vs. GMI results presented in Fig. 7 suggested that for the high SNRs considered in this work, the GMIs achievable using GS-2048 QAM began to saturate. Experimentally, GS-2048 QAM was measured to achieve a gap to capacity of 0.65 b/4D-sym in the back-to-back system and 0.55 b/4D-sym after 100 km of transmission. The testing conducted with our gradient descent optimiser on 2048 QAM and below for a range of lower SNRs indicated that GS unsaturated formats can consistently achieve gaps to capacity of 0.2 b/4D-sym or better. This suggests that up to 0.45 and 0.35 b/4D-sym could be recovered by using GS-4096 QAM over GS-2048 QAM for the back-to-back and transmission cases, respectively. However, the computation time required to optimise constellations of 4096 points or more is currently computationally infeasible for our optimiser. Therefore, future work must develop highly efficient geometric shaping algorithms to allow for fast and flexible optimisations of very high-order QAM formats.

3. The impact of GAWBS was modelled to decrease the maximum SNR of our system by 0.4 dB after 100 km of transmission. GAWBS is, in principle, a correctable form of interference for fully coherent transmission links, and research into DSP compensation techniques is ongoing [50,58]. The inclusion of a successful mitigation technique could recover up to 0.2 b/4D-sym for our system when operating at the optimal experimental SNR of 27.5 dB.

4. The fixed frame size of $N_f = 2^{16}$ used in this work (limited by finite DAC memory) meant that the pilot sequence N_s was non-negligible, resulting in a pilot OH of 4.64%. Under the limit of an infinitely long frame size, the pilot OH is dictated only by the CPE pilot insertion rate $1/N_c$; see Eq. (1) (assuming an otherwise static channel). For the case where $N_c = 32$, as used in this work, this represents a pilot OH of 3.13%. This difference in OH of 1.51% represents a penalty of ~0.25 b/4D-sym for the back-to-back and transmission

Optics EXPRESS

results achieved in this work and increases as any other performance improvements are achieved.

The above information rate penalties add up to 1.2 b/4D-sym in the back-to-back system and 1.3 b/4D-sym after 100 km of transmission. Mitigating these penalties could therefore allow the system presented in this paper to reach an AIR of 19.2 b/4D-sym in the back-to-back system and 18.2 b/4D-sym after 100 km of transmission.

4. Conclusion

We have proposed a pilot-aided digital signal processing (DSP) chain, in combination with high-order geometric constellation shaping, to increase the achievable information rates (AIRs) of standard intradyne transmission systems. The DSP chain was evaluated using 64, 256, 1024, and 2048 QAM, and compared with geometrically-shaped (GS) 1024 and 2048 QAM, designed through gradient descent to maximise the supported information rate at high SNRs. By operating at 15 GBd while using the pilot-aided DSP, the phase noise and electronic jitter contributions were balanced, allowing our system to reach back-to-back and transmission SNR values of 29.5 and 27.5 dB, respectively. At an SNR value of 27.5 dB, GS-2048 QAM was demonstrated to minimise the gap to capacity and offer a higher information rate than GS-1024 QAM; GS-2048 QAM is the highest reported GS constellation cardinality for an optical fibre channel reported to date. By maintaining a pilot overhead (OH) of less than 5%, we demonstrated an AIR of 18.0 b/4D-sym in the back-to-back system and 16.9 b/4D-sym after 100 km of transmission after subtracting the pilot OH. These represent the highest AIR values demonstrated using conventional intradyne detectors, 65 kHz linewidth lasers and 8-bit electronics and show the feasibility of using pilot-aided GS high-order QAM to create low complexity, high-AIR transmission systems. The residual phase noise was identified as a key limitation, and methods for its mitigation were suggested.

Funding. Royal Academy of Engineering; Engineering and Physical Sciences Research Council (EP/R035342/1).

Acknowledgements. Support for this work under the UK EPSRC Programme Grant TRANSNET is gratefully acknowledged. D. Lavery and L. Galdino thank the Royal Academy of Engineering for support under the Research Fellowship scheme, and T. Gerard thanks Microsoft Research for support under the PhD Scholarship Programme.

Disclosures. The authors declare no conflicts of interest.

References

1. C. Laperle and M. OSullivan, "Advances in high-speed DACs, ADCs, and DSP for optical coherent transceivers," J. Lightwave Technol. **32**(4), 629–643 (2014).
2. R. Maher, A. Alvarado, D. Lavery, and P. Bayvel, "Increasing the information rates of optical communications via coded modulation: a study of transceiver performance," Sci. Rep. **6**(1), 21278 (2016).
3. K. Kikuchi, "Characterization of semiconductor-laser phase noise and estimation of bit-error rate performance with low-speed offline digital coherent receivers," Opt. Express **20**(5), 5291–5302 (2012).
4. X. Chen, S. Chandrasekhar, S. Randel, W. Gu, and P. Winzer, "Experimental quantification of implementation penalties from limited ADC resolution for Nyquist shaped higher-order QAM," in *2016 Optical Fiber Communications Conference and Exhibition (OFC)*, (2016), p. W4A.3.
5. S. Varughese, J. Langston, V. A. Thomas, S. Tibuleac, and S. E. Ralph, "Frequency dependent ENoB requirements for m-QAM optical links: An analysis using an improved digital to analog converter model," J. Lightwave Technol. **36**(18), 4082–4089 (2018).
6. L. Galdino, D. Semrau, D. Lavery, G. Saavedra, C. B. Czegledi, E. Agrell, R. I. Killey, and P. Bayvel, "On the limits of digital back-propagation in the presence of transceiver noise," Opt. Express **25**(4), 4564 (2017).
7. L. Galdino, D. Lavery, Z. Liu, K. Balakier, E. Sillekens, D. Elson, G. Saavedra, R. I. Killey, and P. Bayvel, "The trade-off between transceiver capacity and symbol rate," in *2018 Optical Fiber Communications Conference and Exposition (OFC)*, (2018), p. W1B.4.
8. T. Gerard, D. Semrau, E. Sillekens, A. Edwards, W. Pelouch, S. Barnes, R. I. Killey, D. Lavery, P. Bayvel, and L. Galdino, "Relative impact of channel symbol rate on transmission capacity," J. Opt. Commun. Netw. **12**(4), B1 (2020).
9. Keysight, "M8196A 92 GS/s arbitrary waveform generator, datasheet," [Online] https://www.keysight.com/es/en/assets/7018-04911/data-sheets/5992-0971.pdf (2020).

Optics EXPRESS

10. Keysight, "Infiniium Z-Series Oscilloscopes, datasheet," [Online] https://www.keysight.com/gb/en/assets/7018-04251/data-sheets/5991-3868.pdf (2019).
11. D. Qian, E. Ip, T. Wang, M.-F. Huang, and M.-J. Li, "698.5-Gb/s PDM-2048QAM transmission over 3 km multicore fiber," in *39th European Conference and Exhibition on Optical Communication (ECOC 2013)*, (Institution of Engineering and Technology, 2013.
12. A. Matsushita, M. Nakamura, F. Hamaoka, S. Okamoto, and Y. Kisaka, "High-spectral-efficiency 600-Gbps/carrier transmission using PDM-256QAM format," J. Lightwave Technol. **37**(2), 470–476 (2019).
13. K. Schuh, F. Buchali, W. Idler, T. A. Eriksson, L. Schmalen, W. Templ, L. Altenhain, U. Dümler, R. Schmid, M. Möller, and K. Engenhardt, "Single carrier 1.2 Tbit/s transmission over 300 km with PM-64 QAM at 100 GBaud," in *Optical Fiber Communication Conference Postdeadline Papers*, (OSA, 2017).
14. M. Nakamura, F. Hamaoka, A. Matsushita, H. Yamazaki, M. Nagatani, A. Sano, A. Hirano, and Y. Miyamoto, "120-GBaud coded 8 dimensional 16qam WDM transmission using low-complexity iterative decoding based on bit-wise log likelihood ratio," in *Optical Fiber Communication Conference*, (OSA, 2017).
15. M. Nakamura, F. Hamaoka, M. Nagatani, Y. Ogiso, H. Wakita, H. Yamazaki, T. Kobayashi, M. Ida, H. Nosaka, and Y. Miyamoto, "192-Gbaud signal generation using ultra-broadband optical frontend module integrated with bandwidth multiplexing function," in *Optical Fiber Communication Conference Postdeadline Papers 2019*, (OSA, 2019).
16. S. L. Olsson, J. Cho, S. Chandrasekhar, X. Chen, P. J. Winzer, and S. Makovejs, "Probabilistically shaped PDM 4096-QAM transmission over up to 200 km of fiber using standard intradyne detection," Opt. Express **26**(4), 4522 (2018).
17. E. P. da Silva, F. Klejs, M. Lillieholm, S. Iqbal, M. P. Yankov, J. C. M. Diniz, T. Morioka, L. K. Oxenlowe, and M. Galili, "Experimental characterization of 10×8 GBd DP-1024QAM transmission with 8-bit DACs and intradyne detection," in *2018 European Conference on Optical Communication (ECOC)*, (IEEE, 2018).
18. X. Chen, S. Chandrasekhar, J. Cho, and P. Winzer, "Transmission of 30-GBd polarization-multiplexed probabilistically shaped 4096-QAM over 50.9-km SSMF," Opt. Express **27**(21), 29916 (2019).
19. R. Maher, K. Croussore, M. Lauermann, R. Going, X. Xu, and J. Rahn, "Constellation shaped 66 GBd DP-1024QAM transceiver with 400 km transmission over standard SMF," in *2017 European Conference on Optical Communication (ECOC)*, (IEEE, 2017).
20. H. Sun, M. Torbatian, M. Karimi, R. Maher, S. Thomson, M. Tehrani, Y. Gao, A. Kumpera, G. Soliman, A. Kakkar, M. Osman, Z. A. El-Sahn, C. Doggart, W. Hou, S. Sutarwala, Y. Wu, M. R. Chitgarha, V. Lal, H. S. Tsai, S. Corzine, J. Zhang, J. Osenbach, S. Buggaveeti, Z. Morbi, M. I. Olmedo, I. Leung, X. Xu, P. Samra, V. Dominic, S. Sanders, M. Ziari, A. Napoli, B. Spinnler, K. T. Wu, and P. Kandappan, "800G DSP ASIC design using probabilistic shaping and digital sub-carrier multiplexing," J. Lightwave Technol. **38**(17), 4744–4756 (2020).
21. Y. Wakayama, E. Sillekens, L. Galdino, D. Lavery, R. Killey, and P.. Bayvel, "Increasing achievable information rates with pilot-based dsp in standard intradyne detection," in *2019 European Conference on Optical Communication (ECOC)*, (2019), p. W.1.B.5.
22. Y. Koizumi, K. Toyoda, M. Yoshida, and M. Nakazawa, "1024 QAM (60 Gbit/s) single-carrier coherent optical transmission over 150 km," Opt. Express **20**(11), 12508 (2012).
23. S. Beppu, K. Kasai, M. Yoshida, and M. Nakazawa, "2048 QAM (66 Gbit/s) single-carrier coherent optical transmission over 150 km with a potential SE of 153 bit/s/Hz," Opt. Express **23**(4), 4960 (2015).
24. M. Terayama, S. Okamoto, K. Kasai, M. Yoshida, and M. Nakazawa, "4096 QAM (72 Gbit/s) single-carrier coherent optical transmission with a potential SE of 15.8 bit/s/Hz in all-Raman amplified 160 km fiber link," in *Optical Fiber Communication Conference*, (OSA, 2018).
25. S. Okamoto, M. Terayama, M. Yoshida, K. Kasai, T. Hirooka, and M. Nakazawa, "Experimental and numerical comparison of probabilistically-shaped 4096 QAM and uniformly-shaped 1024 QAM in all-Raman amplified 160 km transmission," in *Optical Fiber Communication Conference*, (OSA, 2018).
26. M. Mazur, J. Schroder, A. Lorences-Riesgo, M. Karlsson, and P. A. Andrekson, "Optimization of low-complexity pilot-based DSP for high spectral efficiency 51×24 Gbaud PM-64QAM transmission," in *2018 European Conference on Optical Communication (ECOC)*, (2018), p. Mo4F.2.
27. E. Börjeson, C. Fougstedt, and P. Larsson-Edefors, "ASIC design exploration of phase recovery algorithms for m-QAM fiber-optic systems," in *Optical Fiber Communication Conference (OFC) 2019*, (OSA, 2019), p. W3H.7.
28. J. Cho and P. J. Winzer, "Probabilistic constellation shaping for optical fiber communications," J. Lightwave Technol. **37**(6), 1590–1607 (2019).
29. T. Yoshida, M. Karlsson, and E. Agrell, "Hierarchical distribution matching for probabilistically shaped coded modulation," J. Lightwave Technol. **37**(6), 1579–1589 (2019).
30. B. Chen, C. Okonkwo, D. Lavery, and A. Alvarado, "Geometrically-shaped 64-point constellations via achievable information rates," in *2018 20th International Conference on Transparent Optical Networks (ICTON)*, (2018), pp. 1–4.
31. Z. Qu and I. B. Djordjevic, "Geometrically shaped 16QAM outperforming probabilistically shaped 16QAM," in *2017 European Conference on Optical Communication (ECOC)*, (2017), pp. 1–3.
32. T. Gerard, H. Dzieciol, E. Sillekens, Y. Wakayama, A. Alvarado, R. I. Killey, P. Bayvel, and D. Lavery, "Coded modulation for 100G coherent EPON," J. Lightwave Technol. **38**(3), 564–572 (2020).
33. S. Makovejs, J. D. Downie, J. E. Hurley, J. S. Clark, I. Roudas, C. C. Roberts, H. B. Matthews, F. Palacios, D. A. Lewis, D. T. Smith, P. G. Diehl, J. J. Johnson, C. R. Towery, and S. Y. Ten, "Towards superior transmission

Optics EXPRESS

performance in submarine systems: Leveraging UltraLow attenuation and large effective area," J. Lightwave Technol. **34**(1), 114–120 (2016).
34. A. Alvarado, E. Agrell, D. Lavery, R. Maher, and P. Bayvel, "Replacing the soft-decision FEC limit paradigm in the design of optical communication systems," J. Lightwave Technol. **33**(20), 4338–4352 (2015).
35. B. Chen, Y. Lei, D. Lavery, C. Okonkwo, and A. Alvarado, "Rate-adaptive coded modulation with geometrically-shaped constellations," in *2018 Asia Communications and Photonics Conference*, (2018), p. S3K.5.
36. P. W. Berenguer, M. Nolle, L. Molle, T. Raman, A. Napoli, C. Schubert, and J. K. Fischer, "Nonlinear digital pre-distortion of transmitter components," J. Lightwave Technol. **34**(8), 1739–1745 (2016).
37. R. Kudo, T. Kobayashi, K. Ishihara, Y. Takatori, A. Sano, and Y. Miyamoto, "Coherent optical single carrier transmission using overlap frequency domain equalization for long-haul optical systems," J. Lightwave Technol. **27**(16), 3721–3728 (2009).
38. M. Mazur, J. Schröder, A. Lorences-Riesgo, T. Yoshida, M. Karlsson, and P. A. Andrekson, "Overhead-optimization of pilot-based digital signal processing for flexible high spectral efficiency transmission," Opt. Express **27**(17), 24654 (2019).
39. S. Haykin, *Adaptive Filter Theory (4th Ed.)* (Prentice-Hall, Inc., 2002).
40. M. Magarini, L. Barletta, A. Spalvieri, F. Vacondio, T. Pfau, M. Pepe, M. Bertolini, and G. Gavioli, "Pilot-symbols-aided carrier-phase recovery for 100-G PM-QPSK digital coherent receivers," IEEE Photonics Technol. Lett. **24**(9), 739–741 (2012).
41. X. Zhou, "An improved feed-forward carrier recovery algorithm for coherent receivers with m -qam modulation format," IEEE Photonics Technol. Lett. **22**(14), 1051–1053 (2010).
42. I. Fatadin, S. J. Savory, and D. Ives, "Compensation of quadrature imbalance in an optical qpsk coherent receiver," IEEE Photonics Technol. Lett. **20**(20), 1733–1735 (2008).
43. A. Spalvieri and L. Barletta, "Pilot-aided carrier recovery in the presence of phase noise," IEEE Trans. Commun. **59**(7), 1966–1974 (2011).
44. M. P. Yankov, L. Barletta, and D. Zibar, "Phase noise compensation for nonlinearity-tolerant digital subcarrier systems with high-order QAM," IEEE Photonics J. **9**(5), 1–12 (2017).
45. H. Dzieciol, G. Liga, E. Sillekens, P. Bayvel, and D. Lavery, "Geometric shaping of 2-D constellations in the presence of laser phase noise," J. Lightwave Technol. **39**(2), 481–490 (2021).
46. M. Ionescu, D. Lavery, A. Edwards, E. Sillekens, L. Galdino, D. Semrau, R. Killey, W. Pelouch, S. Barnes, and P. Bayvel, "74.38 Tb/s transmission over 6300 km single mode fiber with hybrid EDFA/raman amplifiers," in *Optical Fiber Communication Conference (OFC) 2019*, (OSA, 2019), p. Tu3F.3.
47. L. Galdino, A. Edwards, W. Yi, E. Sillekens, Y. Wakayama, T. Gerard, W. S. Pelouch, S. Barnes, T. Tsuritani, R. I. Killey, D. Lavery, and P. Bayvel, "Optical fibre capacity optimisation via continuous bandwidth amplification and geometric shaping," IEEE Photonics Technol. Lett. **32**(17), 1021–1024 (2020).
48. R. M. Shelby, M. D. Levenson, and P. W. Bayer, "Guided acoustic-wave brillouin scattering," Phys. Rev. B **31**(8), 5244–5252 (1985).
49. E. Riverahartling, A. Pilipetskii, D. Evans, E. Mateo, M. Salsi, P. Pecci, and P. Mehta, "Design, acceptance and capacity of subsea open cables," J. Lightwave Technol. **39**(3), 742–756 (2021).
50. M. Paskov, M. A. Bolshtyansky, J. X. Cai, C. R. Davidson, D. G. Foursa, and A. N. Pilipetskii, "Observation and compensation of guided acoustic-wave brillouin scattering in modulated channels," in *Optical Fiber Communication Conference (OFC) 2019*, (OSA, 2019).
51. P. Serena, F. Poli, A. Bononi, and J.-C. Antona, "Scattering efficiency of thermally excited GAWBS in fibres for optical communications," in *45th European Conference on Optical Communication (ECOC 2019)*, (Institution of Engineering and Technology, 2019).
52. D. Semrau, R. Killey, and P. Bayvel, "Achievable rate degradation of ultra-wideband coherent fiber communication systems due to stimulated Raman scattering," Opt. Express **25**(12), 13024–13034 (2017).
53. D. Semrau, G. Saavedra, D. Lavery, R. I. Killey, and P. Bayvel, "A closed-form expression to evaluate nonlinear interference in raman-amplified links," J. Lightwave Technol. **35**(19), 4316–4328 (2017).
54. E. T. S. Institute, "Digital Video Broadcasting (DVB); Second generation framing structure, channel coding and modulation systems for Broadcasting, Interactive Services, News Gathering and other broadband satellite applications; Part 1: DVB-S2," [Online] https://www.etsi.org/deliver/etsi_en/302300_302399/302307/01.02.01_40/en_302307v010201o.pdf (2009).
55. T. Pfau, X. Liu, and S. Chandrasekhar, "Optimization of 16-ary quadrature amplitude modulation constellations for phase noise impaired channels," in *2011 37th European Conference and Exhibition on Optical Communication*, (2011), pp. 1–3.
56. H. Dzieciol, E. Sillekens, and D. Lavery, "Extending phase noise tolerance in UDWDM access networks," in *2020 IEEE Photonics Society Summer Topicals Meeting Series (SUM)*, (2020), pp. 1–2.
57. M. Sales-Llopis and S. J. Savory, "Approximating the partially coherent additive white gaussian noise channel in polar coordinates," IEEE Photonics Technol. Lett. **31**(11), 833–836 (2019).
58. M. Nakazawa, M. Yoshida, M. Terayama, S. Okamoto, K. Kasai, and T. Hirooka, "Observation of guided acoustic-wave brillouin scattering noise and its compensation in digital coherent optical fiber transmission," Opt. Express **26**(7), 9165–9181 (2018).